PROCEEDINGS, 49th Workshop on Geothermal Reservoir Engineering
Stanford University, Stanford, California, February 12-14, 2024
SGP-TR-227

Experiments on the Precipitation Behavior of Silicic Acid and Aluminum in Geothermal Water at the Olkaria Geothermal Field, Naivasha, Kenya

Edwin Wanyonyi, Kotaro Yonezu, Takushi Yokoyama and Mutinda Juma

P.O Box, 785-20117, Naivasha, Kenya

Wedwin.wafula@gmail.com

Keywords: monosilicic acid, polysilicic acid, Al-R, silica gel, polymerization, adsorption

ABSTRACT

At Olkaria Geothermal field, Naivasha, Kenya, silicic acid and aluminum precipitation in geothermal water was investigated through batch experiments and immersion of test pieces in flowing geothermal water. This was done through a polymerization experiment by spectrophotometrically measuring monosilicic acid and reactive aluminum concentrations while their total concentrations were analyzed by ICP OES. In addition, an adsorption experiment was carried out using silica gel to act as a model of silica scale to monitor the adsorption behavior of silicic acid and aluminum on the surface of silica gel in actual geothermal water. The polymerization and adsorption experiment results are presented from three sites, OW 38 and OW 24 in the Olkaria east sector and OW 915A in the Olkaria domes. The concentration of Si-M and Si-T decreased rapidly in the first 20 minutes of the experiments, signifying rapid M-P interactions. The concentration of Al-R also rapidly decreased during this period, showing the reaction of a mononuclear aluminum species, in this case, aluminum hydroxide with silicic acid (Due to high pH, aluminum hydroxide is formed instead of alumino-silicic acid), which increased the rate of precipitation of silica. A graphing of this data based on the rate law equation showed that the reactions were of second order, which confirms that probably two first-order reactions could be prominent here: Aluminium hydroxide reaction with silicic acid and the condensation polymerization of monosilicic acid. Fe was seen not to influence the precipitation rate in these experiments as the concentration was constant in all the experiments. Large-sized colloids were also seen to be forming at an early stage via aggregation of the nano colloids that rapidly formed at this highly alkaline condition. Molecular deposition was evidenced by high silica deposition in a very short time on test pieces that were placed on the two-phase sampling valves.

1. INTRODUCTION

Silica is one of the most abundant materials on earth and one of the most common deposits that form from geothermal water during electricity production. This has made it one of the biggest problems of geothermal utilization. Therefore, several studies have been conducted in many geothermal fields across the world with the aim of understanding the mechanisms of silica deposition as well as efficient and economical ways of mitigating its occurrence, e.g. (Gunnarsson and Arnórsson, 2005, Caroll et al. 1998). Silica scaling usually can occur as direct deposition of colloidal material onto surfaces or can go through a nucleation process, which usually will determine the nature or morphology of the scale deposits that form. The nature of monosilicic acid (H_4SiO_4) is such that when it is supersaturated in solution, it's very thermodynamically unstable, which results in polymerization, which is a condensation process involving $Si(OH)$ groups giving rise to coherent molecular units that gradually increase in size and number (Iler, 1979, Chan, 1989). This condensation reaction of monomer species is catalyzed by OH^- as expressed in equation (1) below.

$$2Si(OH)_4 \xrightarrow{OH^-} (HO)_3SiOSi(OH)_3 + H_2O \quad (1)$$

This process is known to be influenced by many parameters, including pH, temperature, ions in solution, salinity, and the nature of the deposition surface. Incidences of scaling have been previously reported in Olkaria by (Opondo, 2007; Wanyonyi et al., 2023), where scaling has been seen on two-phase pipelines, flash separators, brine lines and silencers. However, no substantial experiments have been done to characterize the process of silica precipitation through polymerization experiments in Olkaria. It is well known that even though it is clear to understand and predict the thermodynamics of silica deposition, the kinetics are much more complex and are affected by various other physical factors and operational conditions like changing flow rates, fluid turbulence, and particle sizes, among others (Rothbaum and Rohde, 1979). In addition, most experiments done by other authors have either been in the laboratory or done at neutral to low pH conditions, outside the conditions experienced in Olkaria, a highly alkaline environment. Hingston and Raupach (1967) saw that monomeric silica was firmly and rapidly adsorbed onto the surfaces of hydrous aluminum oxide, while (Yokoyama et al.1982) postulate that rapid monosilicic to polysilicic interactions could occur at about pH 9 due to adsorption of monosilicic acid on aluminum hydroxide. Therefore, to understand the polymerization of silicic acid and aluminum in Olkaria geothermal water, we conducted several experiments at different sites in Olkaria. This study gives the summarized results of those experiments.

2. OLKARIA GEOTHERMAL FIELD

The Olkaria geothermal field is a high-temperature geothermal field located on the floor of the central segment of the Kenyan Rift System, about 120 km northwest of Nairobi city within the Greater Olkaria Volcanic Complex, a young complex (~ 20 Ma) associated with quaternary volcanism and eruption of peralkaline rhyolites (Omenda, 1998; Macdonald et al., 2008). The field is the site for electricity production by the Kenya Electricity Generating Company, which currently has an installed capacity of 799 Mwe, with other geothermal

power plants in advanced feasibility stages. The main lithological units in Olkaria are the Mau tuffs, Plateau trachytes, Olkaria basalts and upper Olkaria volcanics. The rocks occurring on the surface are mainly rhyolite flows and pyroclastic deposits, while trachytes are the primary reservoir rock in Olkaria.

2.1 System Configuration of the Olkaria Geothermal Field

About 125 wells, including production, reinjection, and monitoring wells, are currently in operation at Olkaria, mostly drilled to depths of 3000 m. The current generation capacity of 799 Mwe is supported by six single flash condensing type conventional power plants: Olkaria I (45 MW), Olkaria II (105 MW), Olkaria IV (140 MW), Olkaria I unit 4 & 5 (140 MW) and Unit 6 (83.3 MW) and Olkaria V (158 MW) and 14 wellhead units (88.5 MW). The production wells listed here have varying enthalpy; very high enthalpy wells (>2500 kJ/kg) while some wells at lower enthalpies of (<1800 kJ/kg). The steam field system is also varied, with Olkaria IAU, Olkaria IV, and Olkaria V being operated at 11 bar while Olkaria II and Olkaria I are at about 6 bar. In the current system, some wells are being separated in single flash separators, especially the older steam field at Olkaria I and II, while the newer system is designed such that several wells share a common separator, creating a scenario of mixing of geothermal water within these separator stations. The separated brine is connected directly to the hot reinjection wells while all steam is taken to the power plants. This process diagram is shown in Figure 1 below.

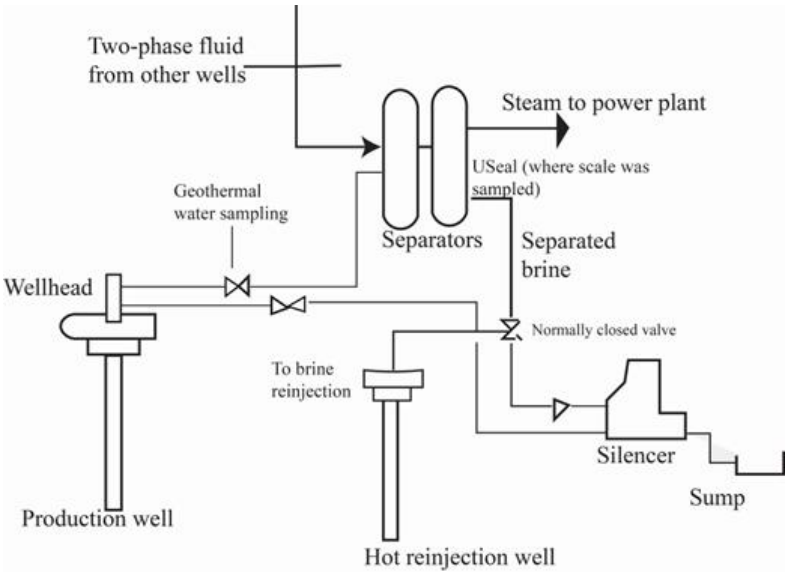

Figure 1: The configuration of the Olkaria Geothermal steam field system

2.1 Scaling condition at Olkaria Geothermal Field

As already seen, several factors play a role in the polymerization process, with the main factors that can be evaluated being pH, SSI and ions in solution. The fluid pH in Olkaria at the wellhead ranges from about 8.5 on the lower side to highs of about 10.5. The impact of pH on polymerization and the overall process of scaling has to do with the ionization effect high pH has on silicic acid (Flemming and Cerar, 1982), leading to the existence of both the silicate ion and the monomer in the pH ranges 9 - 10.7. (Iler, 1979), All silica dissolves above this pH range to form the silicate as per equations (2) and (3) below.

$$Si O_2 + 2H_2O = Si(OH)_4 \quad (2)$$

$$Si(OH)_4 + OH^- = HSiO_3^- + 2H_2O \quad (3)$$

This means, therefore, for the geothermal water in Olkaria, both the silicic and silicate ion coexist, and with the temperature of operation at between 150-190°C (Wanyonyi et al., 2023), reported a ratio of 10.2:1 and 9.1:1. In terms of other, ions Al and F have been seen to exert some influence on the polymerization behavior of silicic acid. In the current experiment, we considered the effect aluminum has on polymerization. Based on this operation temperature, the silica saturation index (SSI) in Olkaria is likely to take the form shown in figure 2 below, which also considers SSI of amorphous aluminum silicate as per (Gallup, 1998).

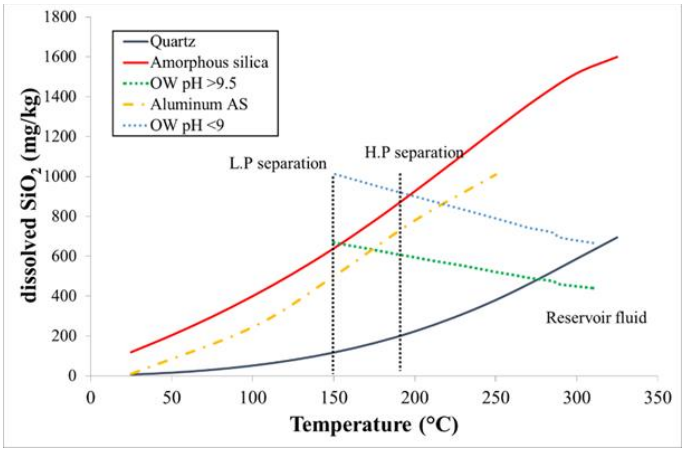

Figure 2: Solubility curves of quartz, amorphous silica and aluminous amorphous silica (Gallup, 1998) as a function of temperature: the silica concentration in the aquifer initially in equilibrium with quartz followed by high-pressure separation at 11 bar and low-pressure separation at 6 bar. One well is a well at pH >9.56, and another at pH < 9.

3. METHOD

3.1 Sampling and Sampling Sites

For this study, we conducted several experiments at the Olkaria geothermal field, including production wells, flash separators, weir boxes, and hot reinjection wells. However, we share results from three sites in this paper. The experiments were designed to ensure a wide range of well characteristics like pH, temperature, salinity, enthalpy and initial SiO_2 concentration were covered. The water samples were collected from the weir box at OW 24 and from the two-phase pipeline at OW 38 and OW 915A. At the two-phase pipeline, a webre separator was used to collect the geothermal water sample following the method of Ólafsson and Armansson (2006), with the sampling point located about 1.5 m from the well head-steam pipe junction. At the weir box, a plastic scoop was used to draw the geothermal water after thorough rinsing with the geothermal water sample at least three times. The samples were rapidly collected in vacuum flasks to maintain the temperature, and the samples were moved to a temporary laboratory adjacent to the sampling sites where the polymerization and adsorption experiment was conducted. Table 1 below shows the sites and the physical characteristics during sampling.

Table 1: Physical characteristics of the wells at the time of sampling

No.	Well, ID.	Sampling point	pH	Temp. (C)	Enthalpy kJ/kg	Mass flow/brine flow (t/hr.)
1	OW 915A	Two-phase line	10.03	190	2430	29/4.5
2	OW 38	Two-phase line	8.34	190	2738	149.9/3
3	OW 24	Weir box	9.7	90	2552	91/8.9

3.2 Experimental

Two experiments were conducted simultaneously using the sampled geothermal water as batch experiments in 1L polyethylene bottles, which were immersed in a thermostatic bath maintained at 85°C. Once the water was collected, it was immediately transferred into the 1L bottle that was acting as the reaction vessel. The experiment was conducted for 90 minutes with samples extracted at intervals of 0, 5, 10, 15, 20, 30, 45, 60, 75 and 90 minutes. At each sampling time, 30-50 ml of sample was extracted using an ADVANTEC 50 ml syringe and filtered through an ADVANTEC 0.45 µm cellulose acetate membrane filter, and the samples stored in a 50 ml polyethylene bottle pre-treated with 0.5 ml of 1M HCl to prevent any further polymerization after sampling. The two experiments involved a polymerization experiment to check the rate of polymerization while the other experiment was conducted as a model in which 1g of a CM-D-50-1000AW Micro sphere silica gel was added to the geothermal water to act as a model of silica particles in order to observe the adsorption of both aluminum and silica with the surface of this gel. The concentration of monomeric silica (Si-M), total silica (Si-T), reactive aluminum (Al-R) and total aluminum (Al-T) were analyzed in this set of samples. In order to characterize the deposits that formed at the early stage, 5 SUS test pieces were also immersed in the weir flow at OW 24 for a period of 5 hours and 42 days, with a test piece being removed at each hour and after every six days, while at OW 38 a test piece was exposed to the two-phase flow line, from a holder hanging from the two-phase pipeline for a period of ten days, with a piece removed after every 2 days. Figure 3 below shows the schematic of these experiments.

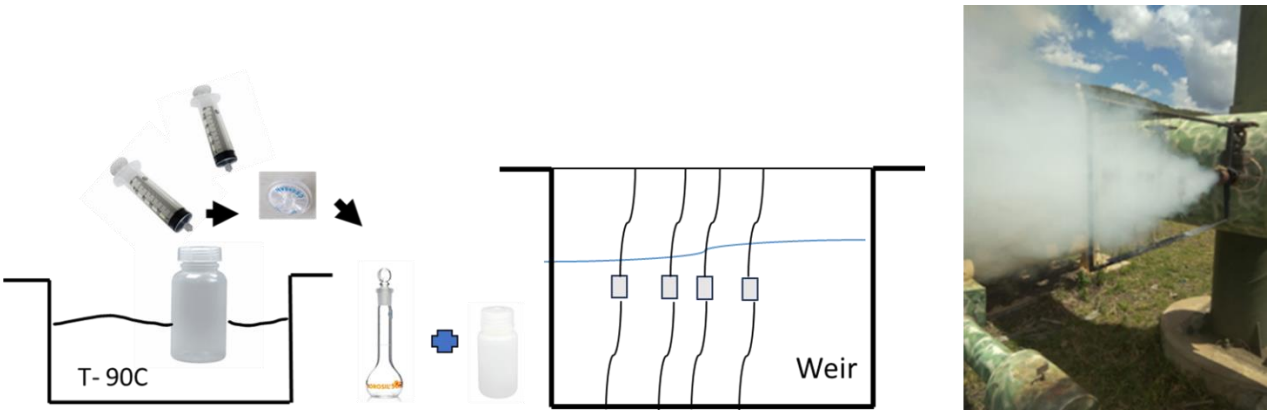

Figure 3: Schematic diagram (left) of the polymerization set-up, (center) test piece immersion in weir box and (right) test piece exposure to flow at a two-phase pipeline at OW 38.

3.2 Analysis

The concentration of monomeric silica was analyzed based on the reaction with molybdic acid to give the yellow silicomolybdic acid using a HACH-DR-900 portable spectrophotometer at an absorbance of 400 nm. Al-R is a ferron (7-iodo-8-hydroxyquinoline-5 -sulfonic acid) reactive aluminum, which was also analyzed using the HACH-DR-900 portable spectrometer at an absorbance of 370 nm. The concentration of total silicic acid (Si-T) and total aluminum (Al-T) was measured by Inductively coupled plasma atomic emission spectroscopy (ICP-AES) using a Perkin-Elmer Optima 5300DV while the concentrations of major elements Na, K, Ca, Mg, Li, F, Cl and SO_4 were determined by Ion Chromatography at the laboratory of Economic Geology and Energy Resources, Kyushu University. The particle sizes in the samples during the polymerization experiment were analyzed by Dynamic light scattering (DLS) using a Malvern Zeta Sizer DLS machine, while the chemistry of colloids on the test pieces was analyzed by SEM-EDX.

3.3 Numerical methods

Geochemical modeling was conducted with the help of The WATCH speciation program version 2.4 (Bjarnason, 2010) and the Geochemist's Workbench© with thermo.dat database. The amorphous silica solubility of pure amorphous silica was calculated based on the equation by (Fournier and Rowe, 1977)

$$\log C = \frac{-731}{T} + 4.52 \quad (4)$$

Where T is the temperature in kelvin

The silica saturation was taken as $S = \frac{C}{C_e}$ (5)

Where C is the concentration of dissolved silica at a given time, while C_e is the amorphous silica solubility at the given temperature.

The rate of silica precipitation r ($mol\ l^{-1}S^{-1}$) has been estimated by several authors (Rimstidt and Barnes, 1980, Rothbaum and Rohde, 1979, Flemming, 1986, Bohlmann et. al., 1980 and Weres, et. al., 1982).

Rimstidt and Barnes, (1980), considered a first-order equation, which we have considered.

$$r = -\frac{dC_{SiO_2}}{dt} = k[C - C_e] \quad (6)$$

Where $k = k^- \frac{A}{M}$

And k^- is the precipitation constant, A/M is the ratio of the surface area to volume of water available in $^{m^2}/_{kg}$ C is the silicic acid concentration (ppm) and *Ce* is the saturation concentration as per equation (4). The rate coefficient k^- is given as a function of temperature by

$$log k^- = -0.707 - \frac{2598}{T_K} \quad (7)$$

Where T_k is temperature in Kelvin.

The average diameter (ds) of the particles was obtained from the average of the z-average readings from DLS measurements, which in this case was assumed to represent particles of a surface area equal to that of the average surface area of the particles in solution. This size was used to calculate the specific surface area, A_{sp} (M^2/Kg) in solution based on the expression below from Iler (1979).

$A_{sp} = \frac{6\times10^3}{density\times d_s}$ where the density was taken as 1.5 gcm^{-3}, being the average density measured for anhydrous amorphous silica deposits from Olkaria, and ds is the z-average diameter in millimicrons from the DLS measurements.

Bohlmann et. al., (1980), considered a second order fit to their experimental data through packed columns and obtained a rate equation which we also considered.

$$r = k[C - C_e]^2 \quad (8)$$

Where, $k = k^{-}AOH^{0.7}$ (9)

And OH, is the hydroxide ion concentration calculated from pH, C is molal silicic acid concentration and A is as used above.

From the transition state theory as developed by Eyring, (1935) and modelled by (Lasaga, 1981; Ladler and King, 1983), the rates of reaction can be determined if the reaction orders are established. This usually can be determined graphically from the integrated rate law, where the first order integrated rate equation is of the form,

$$Ln[C_t] = -kt + Ln[C_t]_0 \quad (10)$$

It is similar to that of a straight line $y = mx + c$ with slope $-k$, Where k is a reaction rate constant, C_t is the current concentration of the first order reactant and C_0 is the initial concentration of the first order reactant and t is time elapsed since the reaction began. We applied this equation too to test our experimental data.

For the second order reaction, the integrated rate law is as below, and we also applied it to our experimental data.

$$\frac{1}{[C_t]} = kt + \frac{1}{[C_t]_o} \quad (11)$$

Is similar to that of a straight line $y = mx + c$ with slope k with symbols as above. The obtained k value was then used in the equations of the form (6) and (14) to determine the precipitation rates. A first-order reaction was that in which data plotted from initial to final concentration produced a strongly linear graph with a negative slope, while the second-order reaction was that which had a strongly positive linear slope. For this work, we used a dimerization reaction of silicic acid based on equations (12) in the plots for the integrated law and calculation of instantaneous rates.

$$SiO_2.2H_2O \rightarrow H_4SiO_4 \quad (12)$$

The instantaneous reaction rate was determined based on the expression in (14) below.

$$\lim_{\Delta t\to 0} \frac{\Delta[concentration]}{\Delta t} \quad (13)$$

While the overall rate of reaction was based on equation 14 below, considering the second-order reaction.

$$r = kA[C - C_e]^2 \quad (14)$$

With C in molal units and A is the surface area in M^2/Kg.

4. RESULTS AND DISCUSSION

4.1 Chemistry of the Geothermal Water and SSI

Table 2 represents the analytical result of the geothermal water from OW 915A, OW 38 and OW 24. The geothermal water was highly alkaline, which is characteristic of geothermal water from Olkaria. The pH at OW 38 and some of the constituent concentrations were low due to steam dilution due to this well's very high steam fraction, which made it nearly impossible to collect a pure water sample, especially at the two-phase line. Na, K, and Cl concentrations were high, which is characteristic of the Na-Cl alkaline type of geothermal water in this sector of the geothermal field. Fluoride and SiO_2 in the three wells were also high, with fluoride being way above the world average. The high fluoride is usually attributed to the decomposition of fluorite in reservoir rocks because of CO_2 release from the deposition of $CaCO_3$. From the chemical data above, the calculated SSI at both the Steamfield operation pressure and at the temperature of the batch experiment is as shown in table 3 below. The SSI was considered for pure amorphous silica and aluminous amorphous silica. The results showed that the SSI is 1.1 for OW 38 and OW 24 and 1.4 for OW 915A considering a pure amorphous state, while it increased to 1,6 and 1.9 respectively when AAS is considered. (Brown, 2011) suggested that when the SSI is kept below 1.2, then it is unlikely that amorphous silica would be problematic, especially at lower pH. Actual silica deposition was seen in the two phase line at OW 38 which happened after it was operated for a few months after being connected to the steam gathering system before being uprated to 11 bars. This meant that there was more to it than just the SSI condition.

Table 2: Analytical result of the geothermal water

	OW 915A	OW 38	OW 24
Component		Value	
pH/T	10.03/25.2	8.34/25.4	9.7/22.2
Na (ppm)	619.1	115.9	534.1
K (ppm)	199.6	40.3	106.9
Al (ppm)	0.04	0.62	0.64
Fe (ppm)	0.01	0.22	0.1
Cl (ppm)	461	174.2	611
F (ppm)	281.9	63.2	118.1
SO_4 (ppm)	77.7	58.6	94.6
CO_2 (ppm)	264	110	66
SiO_2(T) (ppm)	1216	998	678
Ca (ppm)	0	1	0.71
Mg (ppm)	0	0.26	0.04
Li (ppm)	1.5	0.22	0.98
SSI (AS)	1.4	1.1	1.1
SSI (AAS)	1.9	1.6	1.6

Based on the SSI values above, then it would be probable that AAS was present at this site, hence increasing the SSI and likelihood of deposition. Figure 4 below shows the scale deposition at OW 38.

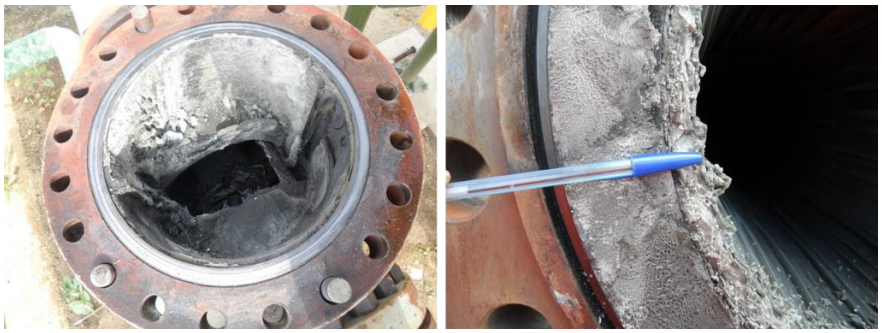

Figure 4: Photographs showing silica scaling, about 2 cm thick, at the two-phase line in OW38 in 2015.

4.2 Polymerization and Precipitation of Silicic Acid and Aluminum

The polymerization and adsorption experiment results are presented from the three sites, OW 38 and OW 24 in the Olkaria east sector and OW 915A in the Olkaria domes. Figures 5, 6, and 7 below show the changes in Si-M and Si-T concentrations over 90 minutes at the three sites. At OW 38, under polymerization, the initial Si-T concentration was 998 ppm while the Si-M was 493 ppm, suggesting that polysilicic particles were already present at the start of the experiment. The Si-T concentration moderately reduced in the first 30 minutes of the experiment to 704 ppm and became nearly constant or reduced just slightly up to the end of the experiment. On the other hand, the Si-M moderately reduced within the first 20 minutes to 418 ppm and then continuously decreased very slowly until it was constant by the 80th minute. Assuming the difference between the Si-T and Si-M to be the concentration of polysilicic acid, then it suffices to say that about 50% of the silica existed as polysilicic particles already at the start and entire experiment period. This sample was taken, as already mentioned, from the two-phase line and later pre-treated with acid to prevent polymerization before analysis, which would suggest that already at the initial two-phase conditions, 11 bars in this case, before sampling, the geothermal water was already undergoing or had undergone significant polymerization to form the polysilicic acid. The filtration during sampling was done with a 0.45 µm membrane; then, it's expected that any particles larger than this size would be filtered out, which is also possibly the case here. The simultaneous reduction in Si-T and Si-M was an indication of monosilicic to polysilicic interactions, as well as possibly polysilicic to polysilicic interactions. Usually, in slow cooling and high-temperature conditions, larger colloids are expected to form, even though these large colloids are usually less stable than the smaller colloids (Iler, 1979). The Si-M decreased much slower after the 20th minute, signifying that the kinetics of molecular deposition were probably slower. The monomer concentration is above the equilibrium solubility of

amorphous silica at the experiment temperature; the instability of large colloids that either react or redissolve to smaller particles could lead to a proliferation of smaller particles again, which are more soluble than amorphous silica. The adsorption experiment had nearly the same pattern as the polymerization experiment at this site, with the main difference being the initial concentration of Si-T, which was slightly lower at 708 ppm. This would suggest that there was a rapid interaction of the polysilicic particles with the surface of the silica gel at the very onset of the experiment, giving credence to the suggestion of more P-P interactions under these conditions, with the M-M being rapid within the well itself to give rise to the high concentration of polysilicic acid at sampling. As already discussed, its thought that at pH greater than 7, the rate of polymerization is generally fast, catalysed by a high presence of hydroxyl surfaces.

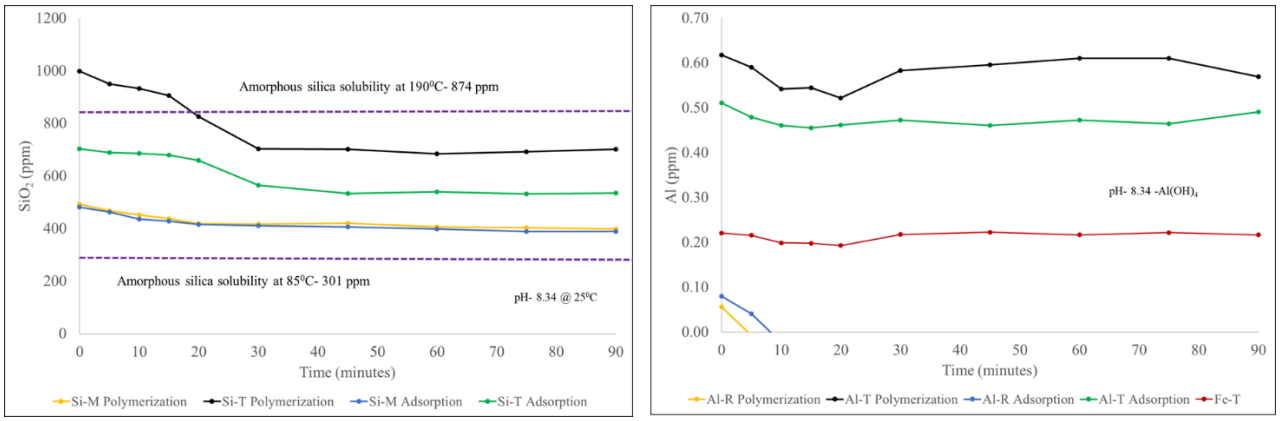

Figure 5: Change in the concentration of total silica (Si-T), monomeric silica (Si-M), total aluminum (Al-T), reactive mononuclear aluminum (Al-R) and total iron (Fe-T) in the polymerization and adsorption experiment at OW 38.

At OW 24, the behavior of both Si-T and Si-M was similar to that at OW 38, with a moderate decrease from onset to the 20th minute and, thereafter slow reduction, then nearly constant to the end of the experiment. In this case, even though the Si-T is higher than Si-M, the magnitude is much lower than in the former. The Si-T during the adsorption experiment was also slightly lower than the polymerization, just as it was in OW 38. This suggests that even though the wells have different concentrations, which is a specific attribute of each well, their behavioral pattern as regards the interaction of silicic particles is essentially the same. At OW 915A, which is located in the Olkaria domes, a different field sector from where the other two wells are located, (East sector), there was some slight difference in the behavior. The Si-T and Si-M reduced rather slowly compared to the other two experiments, but this reduction also happened in the first 20 minutes. The concentration of Si-T was higher than that of Si-M, in concurrence with the earlier proposed presence of a bulk load of polysilicic acid or colloids before the start of the experiment. Like in OW 38, the samples were also taken at the two-phase line, which was at 11 bars. The Olkaria domes represent the area in Olkaria with the highest concentrations of silica as well as some of the highest fluid pH values, which seems to be the case here, too. At a high pH of > 10.01, the ionization of silicic acid had probably occurred within the two phase, and the ratio of $Si(OH)_3O^-$ to $Si(OH)_4$ is high, which could reduce the rate of polymerization as seen in this experiment compared to OW 38 at pH 8.34.

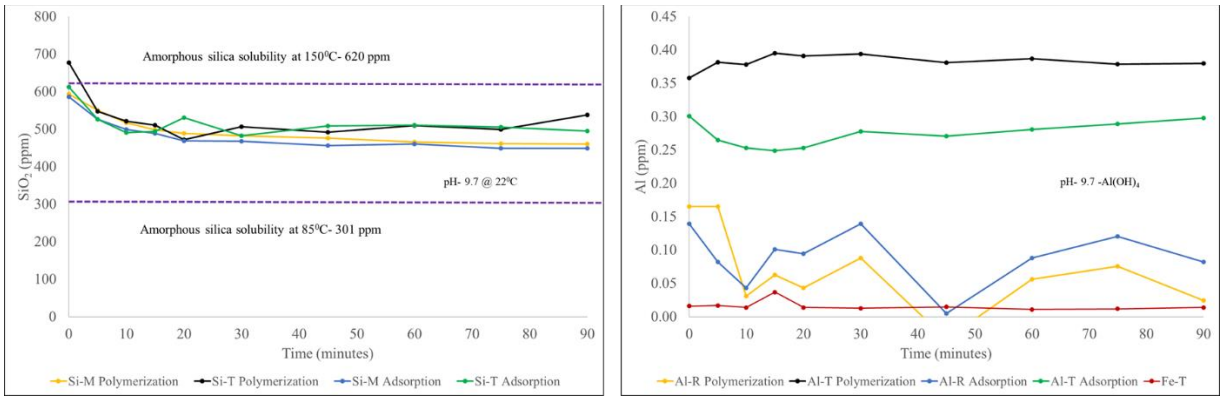

Figure 6: Change in the concentration of total silica (Si-T), monomeric silica (Si-M), total aluminum (Al-T), reactive mononuclear aluminum (Al-R) and total iron (Fe-T) in the polymerization and adsorption experiment at OW 24.

Generally, the wells used, there was indication of rapid polymerization within the two phase zone in the wells forming polysilicic particles at those points even prior to sampling. At high pH, greater than 7, SiO_2 is known to polymerize rapidly to discrete particles that could begin to aggregate, with the monomer decreasing rapidly and oligomers increasing. The highly alkaline fluids, in general, have abundant hydroxyl surfaces that act as catalysts for polymerization, as well as creating a basis for interparticle interactions, hence the development of larger particles. In this case, there were abundant polysilicic to polysilicic interactions after the initial rapid polymerization in the wells that were M-M reactions or interactions with other ions in solution. The kinetics of the molecular deposition are usually guided by the

size of the particles that developed as well as other physical characteristics of the deposition environment like turbulence and fluid flow rates. In addition, at higher pH, there is an increased ionic charge which would be sufficient to reduce collision and aggregation hence minimal polymerization as is the case in OW 915.

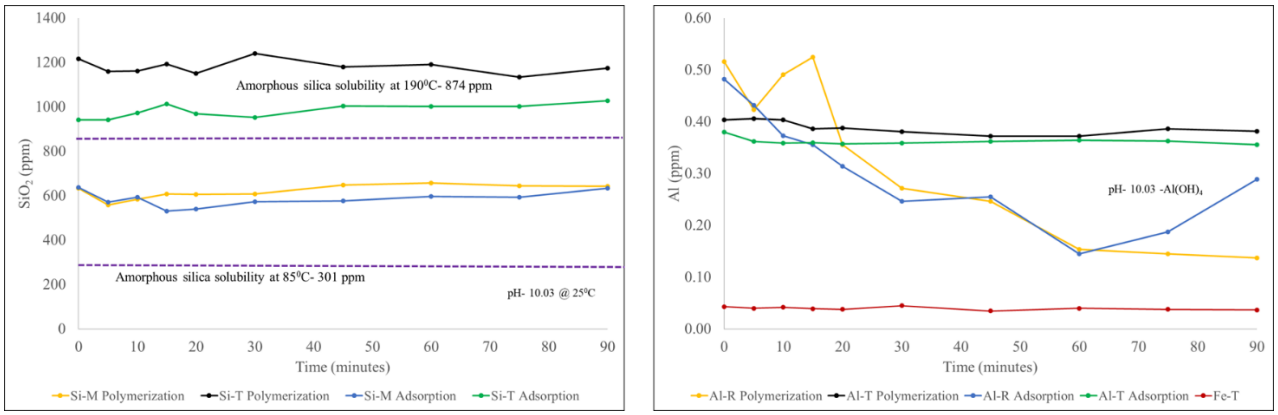

Figure 7: Change in the concentration of total silica (Si-T), monomeric silica (Si-M), total aluminum (Al-T), reactive mononuclear aluminum (Al-R) and total iron (Fe-T) in the polymerization and adsorption experiment at OW 915A.

Figures 5-7 above show the changes in the concentration of total aluminum (Al-T) and reactive aluminum (Al-R) in both the polymerization and adsorption experiments from the three sites. At OW 38, the concentration of Al-T at the onset of the polymerization experiment was 0.62 ppm, while the concentration for Al-R was 0.06 ppm. Al-T slightly decreased from the start of the experiment to the 20th minute, where it was 0.55 ppm, and thereafter slightly increased and maintained constant. Al-R, on the other hand, rapidly decreased from the onset of the experiment to zero. The Al-T in the adsorption experiment was slightly lower than in the polymerization experiment, with an initial concentration of 0.51 ppm and slightly reduced by .02 ppm up to the end of the experiment. The trend was similar in the experiments from the other sites, with the Al-T slightly reducing at the initial stages and remaining reasonably constant to the end of the experiment, while Al-R rapidly decreased from the start of the experiment until the end. In addition, the Al-T was slightly lesser in the adsorption experiment than in the polymerization experiment. Several authors have shown that aluminium species can rapidly incorporate silicic acid, leading to faster deposition of amorphous silica (Ichikuni, 1970; Yokoyama et al., 1993; Gallup, 1997). In addition, the speciation of aluminum has been seen to be pH dependent, and in the case of the Olkaria Geothermal water, the main species is the $Al(OH)_4^-$ due to the alkaline nature of the geothermal water. The rapid decrease in the concentration of Al-R is thought to be due to the incorporation of a mononuclear Al, in this case aluminum hydroxide onto the polysilicic particles which occurs by isomorphous substitution based on results from ^{27}Al MAS NMR by some authors, e.g. (Masunaga et. al, 2020). Because of the high pH in some of the sites here that leads to extreme ionization, that reaction could be between the silicate $Si(OH)_3O^-$ and $Al(OH)_4^-$ forming aluminosilicate. This kind of process has been known to accelerate the rate of silica precipitation from geothermal water. The slight reduction in the Al-T could also signify the presence of aluminum hydroxide precipitate on colloid surfaces, forming conducive sites for Si-M adsorption. The lower concentration of Al-R in the adsorption experiment shows faster aluminum adsorption onto the surface of the silica gel, which was a model of silica colloid particles. Houston, et al. (2008) proposed three reactions relating aluminum with amorphous silica, including sorption of dissolved aluminum, surface precipitation of aluminum hydroxide as well as precipitation of aluminosilicates, while (Yokoyama, 1991) suggested that at high pH greater than 9, there could be precipitation of aluminosilicate on the surfaces of polysilicic acid. In that case, there is the possibility that the slight reductions in Al-T and the Si-T reductions could be related to one of these processes. We are currently conducting ^{27}Al MAS NMR analysis from ion exchange experiments conducted simultaneously with these experiments to give the chemical state of aluminium in these experiments. However, analysis conducted on scale samples deposited from wells located near these experimental sites showed the presence of tetrahedral and octahedral coordinated aluminum. The concentration of total iron (Fe-T) was constant throughout the experiments, precluding the participation of Fe in the polymerization or precipitation of Si from the Olkaria geothermal water but probably as an iron-rich mineral.

4.2 Chemical Characteristics and Size of Colloids

At the same period as the experiments in 4.1 above, additional experiments involving immersion of test pieces in the weir flow and exposure to two-phase fluid flow were conducted. This was done to evaluate the actual molecular deposition behaviour by chemical analysis of the deposits that were formed on the test pieces. The immersion experiment was conducted at the weir box at OW 24 for a five-hour period, with a piece being taken every hour and for 42 days, with a piece removed every five days. At OW 38, the SUS test pieces were exposed to the steam and water flow from the sampling valve for 8 days, with the first pick being done on the fourth day and a piece taken every 2 days thereafter. SEM-EDX was used to determine the morphology as well as weight percent of various elements. Figure 8 shows the secondary electron images of the SUS test pieces as observed under SEM while table 3 shows the chemical composition from EDX analysis. From the EDX analysis of the test pieces from the OW 24 immersion experiment, Si was the most abundant element that deposited within the first one hour at 3.7 wt.% and subsequently increased in the two hour to 14 wt.%. Al was also seen to have an increasing trend from the first one hour to four hour. This increases in element concentration matched the polymerization experiments where the changes in concentration of these two elements were highly correlated, and it goes to show that they were actually the main two players in the precipitation process. In comparison, the SUS pieces from the flow experiment at OW 38 showed high Si deposition within the early days at 96.7 wt.% with Al being the second most abundant element at 0.67 wt.%. This is important since the

sampling point was at the two phase section, and as already discussed, rapid polymerization could be occurring at this zone prior to sampling. These results confirm this early formed colloids pre-existing in the geothermal fluid at the two phase line.

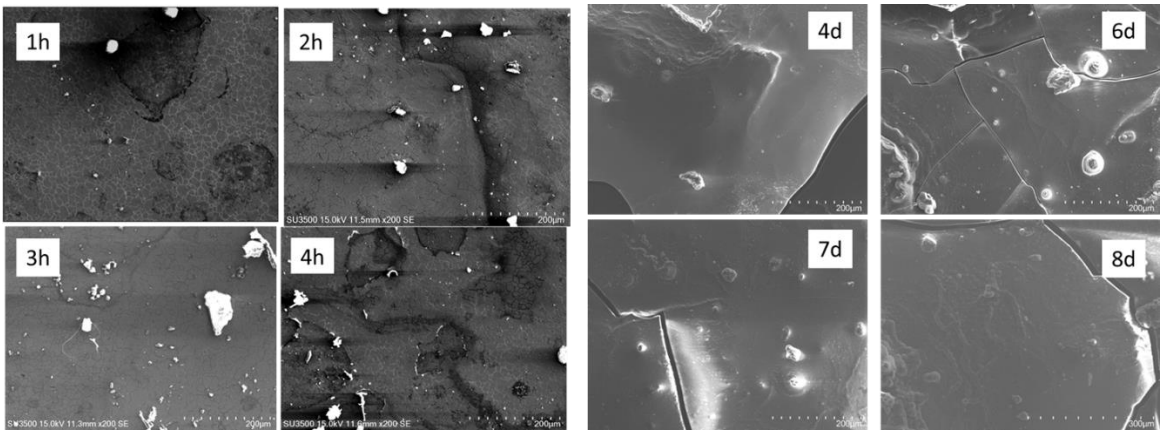

Figure 8: Secondary electron (SE) images from SEM for SUS test pieces immersed in geothermal water at OW 24 for 4 hours (1h-4h) and that exposed to flow at OW 38 for 8 days (4d-8d), showing the colloid deposition.

Table 3: Elemental analysis from EDX on SUS test pieces at OW 24 and OW 38

	Time (hours)			
Element (At%)	1	2	3	4
SUS	OW 24			
Na	0.36	0.45	0.28	0.56
Mg	0.05	0.1	0.05	0
Al	0.07	0.28	0.37	0.32
Si	3.73	14.04	14.8	17.05
K	0.12	0.1	0.17	0.23
Ca	0.1	0.15	0.15	0.2
Cr	17.81	16.1	15.84	15.45
Mn	0.97	0.87	0.65	0.72
Fe	69.35	61.33	61.18	59.16
Ni	7.44	6.58	6.52	6.31
Total	100	100	100	100

	Time (days)					
Element	4	6	7	8	9	10
SUS	OW38					
Na	0.65	0.57	0.63	0.65	0.74	0.6
Mg	0.13	0.1	0.09	0.13	0.09	0.18
Al	**0.65**	**0.78**	**0.62**	**0.77**	**0.81**	**0.74**
Si	**96.75**	**96.18**	**95.01**	**93.98**	**95.9**	**96.52**
K	0.47	0.62	0.43	0.56	0.6	0.51
Ca	0.16	0.15	0.1	0.15	0.12	0.1
Cr	0.25	0.33	0.57	0.65	0.3	0.23
Mn	0	0	0	0	0	0
Fe	0.67	0.98	2.05	2.62	1.04	0.73
Ni	0.27	0.28	0.5	0.49	0.41	0.39

The compatible behaviour of Si and Al in these geothermal waters gives credence to the processes discussed in 4.1 above regarding the interaction of Si and Al during the silica precipitation process. The colloids also gradually increased in size from the 1-hour experiment, where the average diameter of the largest colloid was about 250 nm, then 300-400 nm at two hours, and 500-600 nm at 4 hours, showing growth through nucleation and agglomeration occurs in this geothermal water as well as massive molecular deposition on surfaces as seen from the images in 4d-8d. In the case of OW 38, the initially deposited sheet is subsequently overlain by a layer of spherical colloids, showing that once surfaces are provided, monosilicic acid particles start adsorbing on this already formed surface. The size distribution from the polymerization experiments was measured from the intensity size distribution data measured by DLS. This is usually based on the intensity of light scattered by particles and can be very sensitive to the presence of large particles. Figure 9 below shows the Intensity PSD graphs with the peak size distribution from the analysis of the samples. All the samples analysed for OW 38 and OW 24 had Polydispersity Index (PDI) values between 0.2 and 0.4, which is a mid-range value signifying a narrow range distribution of the particle sizes, especially given that a 450 nm filtration was done for all samples. Usually, in DLS analysis, small particles are known to have rapid fluctuations when the intensity vs time data is plotted while large particles are known to have smoother and less rapid fluctuations. From Figure 9, the size distribution was displayed as a plot of the relative intensity versus the size classes for each sampling time in nanometre (nm) which was logarithmically spaced. From the plot for OW 38, the peaks were centered around 40-50 nm logarithmic with the dispersion also being smooth, which signified the presence of homogenously large sized particles. In the plot of OW 24, there was a little homogeneity in the distribution with the peak fluctuation at 60 nm and 110 nm signifying some large particles but also a number of small particles present. In general, these results matched those seen from SEM where some small sized colloids and large colloids occurred on the surface of test pieces, and also collaborates our prediction from the polymerization experiment about the growth of particles due to the reducing Si-T concentrations during the experiments.

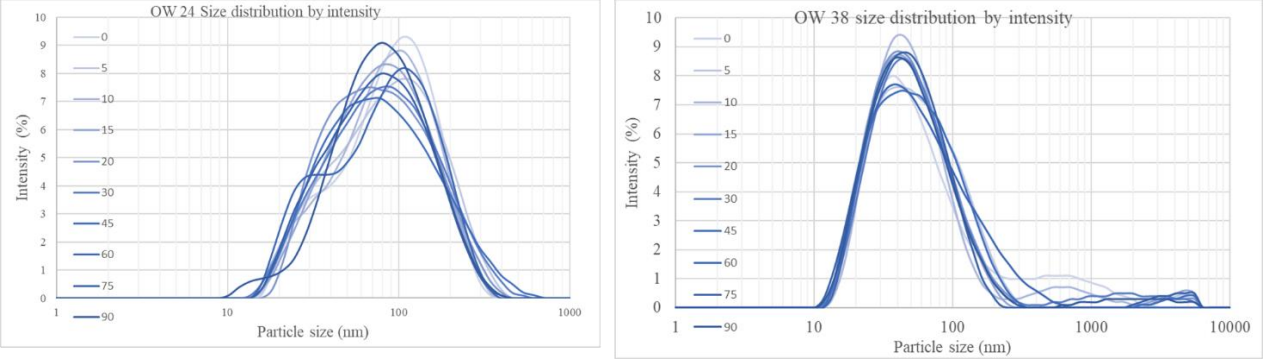

Figure 9: Intensity PSD showing the peak distribution of the size of dissolved particles (<450 nm) at different sampling times during the polymerization experiments at OW 24 and OW 38.

4.3 Kinetic modelling- reaction order and rate of reaction

Many polymerization experiments have been conducted under different experimental conditions worldwide, thereby leading to varying reported data of reaction orders. Based on the current experiment, we examined the possible reaction orders using equations (10) and (11) and guided by the dimerization reaction in equation (12). The first-order and second-order reactions for polymerization and adsorption experiments for OW 24 are shown in Figures 10 and 11 below, and the comparison of the least squares fit from the graphs is shown in Table 4 below. Both runs of the two experiments gave two distinct line segments with two different slopes, similar to Run 2F in Rimstidt and Barnes (1980), who also saw a similar partition from their experiment. From these data, in the polymerization experiment there is a close similarity between the first order and second order reaction based on the R^2 value. However, in the adsorption experiment, the reactions were basically of the second order as the R^2 were > 0.99 compared to < 0.7 for the first order. Therefore, considering the first 20 minutes of the experiment, and especially for the adsorption experiment, then it suffices to consider a second order reaction and the rate constants were therefore based on this consideration in terms of monosilicic acid concentration. But, for comparison purposes, rate determinations were also calculated based on first order reaction rate consideration.

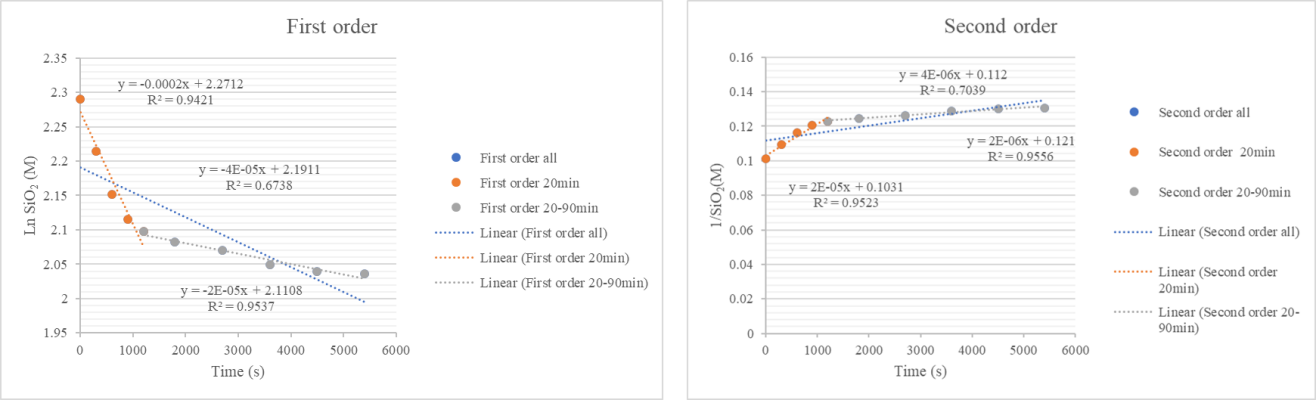

Figure 10: Application of the rate law by graphing the experimental concentration against the first-order and second-order equations to find the reaction order in the OW 24 polymerization experiment.

The fit from 0-20 minutes had the best R^2 value, followed by the fit from the 20-90 minutes that could correspond to two phases or two mechanisms occurring during the experimental duration. Usually, a second-order reaction is one in which the reaction rate depends either on the concentration of one second-order reactant or two first-order reactants. From figure 5 and 6, it was shown that a rapid reaction of monosilicic acid and aluminum hydroxide occurred in the first 20 minutes of the experiment. In addition, figure 5 showed the possible deposition of monomeric silica and polymeric silica from the same solution, given the significant differences in Si-T and Si-M. Thus, the first line fit possibly represents the rapid precipitation of monosilicic acid as a reaction with aluminum hydroxide as well as a first order addition of monomers to the instantly formed discrete polysilicic particles due to high pH, with slow condensation polymerization as catalyzed by the hydroxide ion probably also occurring. The 20-90 minute interval, then would be slow adsorption of monosilicic acid possibly to the formed Al-Si complexes as well as slow aggregation of colloidal silica, and hence the second line fit in the graph.

From the precipitation constants k in Table 4, which were obtained from these integrated rate law graphs, the reaction rates were calculated as shown in Figure 12 below. For OW 24, the second order rates for polymerization and adsorption experiments were nearly matched at initial rates of 1.19E+01 and 1.13E+01 mol $L^{-1}S^{-1}$ respectively, while that calculated based on the Bohlmann model at pH 9.7, A 25 m^2/g and k' 0.12 gave 6.63E+01 kg/mol/min. For the first order rates, those calculated using the Rimstidt and Barnes model gave the lowest initial rate at 8E-02 mol $L^{-1}S^{-1}$, while the experimental first order rate was 1.46E+02 mol $L^{-1}S^{-1}$. The rate of linear growth of amorphous silica as per the Bohlmann prediction equation was 6.9E-02 cm/min. Its therefore probable that the experimental results followed a second

order reaction. In geochemical reactions, the reaction rate is usually defined in order to know the variations that occur with time, changing reactant and product concentrations and in some cases pH or temperature. This could either be the average rate which is usually the average rate of reaction over a given period of time within the entirety of the reaction, or it could be an instantaneous rate, which is that a specific given time in the reaction. Therefore, it's possible to partition the reaction rates in different phases depending on the rate of the disappearance of the reactant vis a vis the rate of appearance of the product.

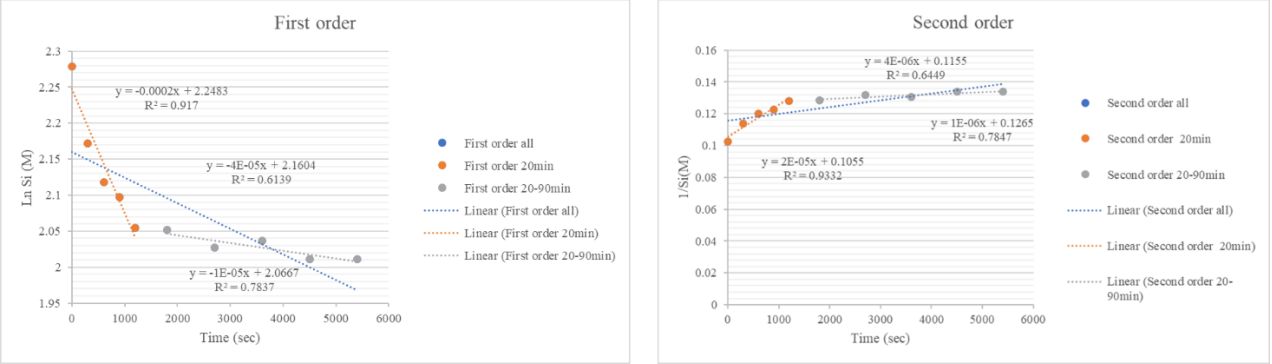

Figure 11: Application of the rate law by graphing the experimental concentration against the first order and second order equations to find the reaction order for OW 24 adsorption experiment.

The results showed a faster rate of reduction in the first minutes of the experiment where subsequent after that the rate reduced and became very slow. This could indicate that once the initial particles have grown to the critical size, then there is a continued growth of the primary colloids and less growth of the primary silicic acid particles until the monomers approach the solubility of the particle. It has been shown that the activation energy required to form new particles is usually larger and hence particles easily adsorb on available surfaces. As such in the later minutes of the experiments, it seemed more adsorption is occurring than any condensation reactions. The rate sometimes slows down once the concentration in solution reaches or approaches the equilibrium solubility of amorphous silica, yet in our case from the polymerization graphs, we noted the reactions had not crossed the amorphous silica solubility at the temperature of experiment.

Table 4: Comparison of linear regression fits and k values for first order and second order reactions.

Well	Temp	First order				Second order			
	85C	Polymerization		Adsorption		Polymerization		Adsorption	
	Time	k	R^2	k	R^2	k	R^2	k	R^2
OW 24	0-20 min	2.00E-04	0.9421	2.00E-04	0.917	2.00E-05	0.9523	2.00E-05	0.9332
pH-9.7	20-90 min	2.00E-05	0.9537	1.00E-05	0.7837	2.00E-06	0.9556	1.00E-06	0.7847
	0-90 min	4.00E-05	0.6738	4.00E-05	0.6139	4.00E-06	0.7039	4.00E-06	0.6449
OW 38	0-20 min	1.00E-04	0.9902	1.00E-04	0.9735	2.00E-05	0.9911	2.00E-05	0.9717
pH-8.34	20-90 min	1.00E-05	0.8246	2.00E-05	0.9422	2.00E-06	0.9556	3.00E-06	0.9421
	0-90 min	3.00E-05	0.7309	3.00E-05	0.7743	4.00E-06	0.7515	5.00E-06	0.7978

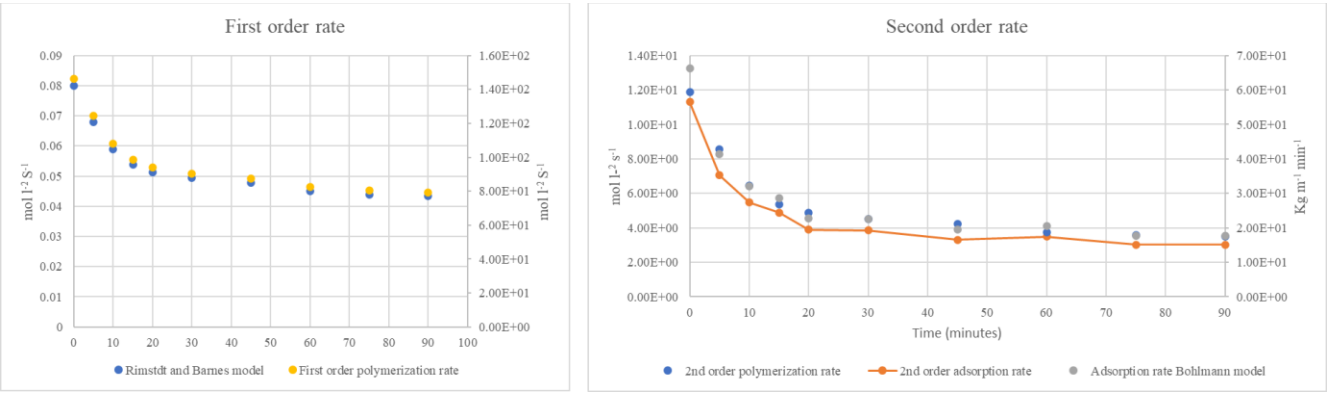

Figure 12: First and second order rates of polymerization of monosilicic acid as determined using precipitation constants from batch experiments conducted at 85°C and at the original pH of the geothermal water.

5. CONCLUSION

The polymerization and adsorption experiment results are presented from three sites, OW 38 and OW 24 in the Olkaria east sector and OW 915A in the Olkaria domes. The concentration of Si-M and Si-T decreased rapidly in the first 20 minutes of the experiment, signifying the M-P interactions rapidly occurring at this time. The concentration of Al-R also rapidly decreased during this period showing the reaction of the mononuclear species in this case aluminum hydroxide with silica acid could be increasing the rate of precipitation of silica. A graphing of this data based on the integrated rate law equation, showed that the reactions were of second order, which confirms that at least two first order reactions could be prominent here, that of Al adsorption on silicic acid in addition to the condensation polymerization of monosilicic acid. Fe was seen to not influence the rate of precipitation in these experiments as the concentration was constant throughout. Large sized colloids were also seen to be forming at an early stage via aggregation of the nano colloids. Molecular deposition was evidenced from high silica deposition in a very short time on test pieces exposed on the two phase pipeline.

6. ACKNOWLEDGEMENT

We would like to thank the Japan International Cooperation Agency (JICA) KIZUNA program, LENGO project under SATREPS (led by Prof. Fujimitsu, Kyushu University) and the Kenya Electricity Generating Company (KenGen) PLC for supporting this research.

REFERENCES

Ármannsson, H., and Ólafsson, M., 2006. Collection of geothermal fluids for chemical analysis. ÍSOR – Iceland GeoSurvey, Reykjavík, report ISOR-2006/101, pp 17.

Bjarnason, J.O., 2010. The chemical speciation program WATCH. Version 2.4 Iceland GeoSurvey. Accessible at. http://www.hydrothermal.is/software.

Bohlmann, E. G., Mesmer, R. E. and Berlinski, P., 1980. Kinetics of silica deposition from simulated geothermal brines. Soc. Pet. Engng J. 20,239-248.

Brown, K., Thermodynamics and Kinetics of Silica Scaling, Proceedings International Workshop on Mineral scaling, Manila Philippines, 25-27 May (2011).

Carroll, S., Mroczek, E., Alai, M., Ebert, M., 1998. Amorphous silica precipitation (60 to 120 °C): comparison of laboratory and field rates. Geochim. Cosmochim. Acta 62, 1379–1396

Chan, S.H., 1989. A review on solubility and polymerization of silica. Geothermics 18 (1/ 2), 49–59

Dixit, C., Bernard, M. L., Bernard, S., Andre, L., Gaspard, S., 2016. Experimental study on the kinetics of silica polymerization during cooling of the Bouillante geothermal fluid (Guadeloupe, French West Indies), Chemical Geology, 442, 97-112.

Eyring, H., 1935. J. Chem. Phys.,3, 107

Fleming, B. A. (1986) Kinetics of reaction between silicic acid and amorphous silica surfaces in NaC1 solutions. J. Colloid Interface Sci. 110, 40-64

Fleming, B. A., Crerar, D. A., 1982. Silicic acid ionization and calculation of silica solubility at elevated temperature and pH. Application to geothermal fluid processing and reinjection. Geothermics, 11, 15-29.

Fournier, R.O., Rowe, J.J., 1977. The solubility of amorphous silica in water at high temperatures and high pressures. Am. Mineral. 62, 1052–1056.

Gallup, D. L., 1997. Aluminum silicate scale formation and inhibition: Scale characterization and laboratory experiments. Geothermics, 26, 483-499.

Gallup, D.L., 1998. Aluminum silicate scale formation and inhibition (2): scale solubilities and laboratory and field inhibition tests. Geothermics 27 (4), 485–501.

Gunnarsson, I., Arnórsson, S., 2005. Impact of silica scaling on the efficiency of heat extraction from high-temperature geothermal fluids. Geothermics 34, 320–329

Hingston, F. J. and Raupach, M. 1967. Aust. J. Soil. Res., 5(2), 295

Houston, J. R., Herberg, J. L., Maxwell, R. S., Carroll, S. A., 2008. Association of dissolved aluminum with silica: Connecting molecular structure to surface reactivity using NMR, Geochim. Cosmochim. Acta, 72, 3326-3337.

Ichikuni, M., 1970. Incorporation of aluminum and iron into siliceous sinters. Chem. Geol., 6, 273-279.

Iler, R.K., 1979. The Chemistry of Silica. Solubility, Polymerization, Colloid and Surface Properties and Biochemistry. John Wiley and Sons, New York (866 p).

Laidler, K., Christine, K., 1983. The Development of Transition-State Theory. J. Phys. Chem. 87, 2657-2664.

Lasaga, A.C., 1981. Transition state theory. In: Lasaga, A.C., Kirkpatrick, R.J. (Eds.), Kinetics of Geochemical Processes Rev. Mineral. 8, 1–67

Macdonald, R., Black, H.E., Fitton, J.G., Marshall, A.S., Nejbert, K., Rodgers, N.W., and Tindle, A.G., 2008. The roles of fractional crystallization, magma mixing, crystal mush remobilization, and volatile-melt interactions in the genesis of a young basalt-peralkaline rhyolite suite, the Greater Olkaria volcanic complex, Kenya Rift Valley. J. Petrol., 1515-1547.

Masunaga, K. Y., Tasaka, Y., Inoue, H., Yonezu, K., Kiyota , Y., Watanabe, K., Yokoyama, T., 2020. Chemical state of aluminum in geothermal water. Proceedings World Geothermal Congress 2020, Reykjavik, Iceland (2020 + 1).

Omenda, P.A., 1998. The geology and structural controls of the Olkaria geothermal system, Kenya. Geothermics, 27-1, 55-74.

Opondo, K.M., 2007. Corrosive Species and Scaling in Wells at Olkaria, Kenya and Reykjanes, Svartsengi and Nesjavellir, Iceland. Report 2 in Geothermal training in Iceland 2006. UNU-GTP, Iceland, 165-188.

Rimstidt, J.D., Barnes, H.L., 1980. The kinetics of silica-water reactions. Geochim. Cosmochim. Acta 44, 1683–1699

Rothbaum, H.P., Rohde, A.G., 1979. Kinetics of silica polymerization and deposition from dilute solutions between 5 and 180 °C. J. Colloid Interface Sci. 71 (3), 533–559.

Wanyonyi, E., Yonezu, K., Yokoyama, T., Imai, A., Opondo, K., and Koech, K. 2023. Geochemical study on the deposition of silica scale at Olkaria well OW-35: A key to understanding the formation mechanisms of silica scale at the Olkaria Geothermal Field, Kenya. Geothermics, 117.

Weres, D., Yee, A. and Tsao, L., 1982. Equations and type curves for predicting the polymerization of amorphous silica in geothermal brines. Soc. Pet. Engng J. 22, 9 16.

Yokoyama, T., Nakamura, O., Tarutani, T., 1982. Polymerization of silicic acid adsorbed on aluminum hydroxide. Bull. Chem. Soc. Jpn. 55 (4), 975–978.

Yokoyama, T., Sato, Y., Maeda, Y., Tarutani, T., Itoi, R., 1993. Siliceous deposits formed from geothermal water I. The major constituents and the existing states of iron and aluminum. Geochem., Jour., 27, 375-384.

Yokoyama, T., Takahashi, Y., Tarutani, T., 1991. Retarding and accelerating effects of aluminum on the growth of polysilicic acid particles. J. Colloid & Interface Sci., 141, 559-563